

A fast recursive coordinate bisection tree for neighbour search and gravity

Emanuel Gafton^{*} & Stephan Rosswog
Jacobs University Bremen, Campus Ring 1, 28759, Bremen, Germany

Accepted 2011 July 28. Received 2011 July 14; in original form 2011 May 12

ABSTRACT

We introduce our new binary tree code for neighbour search and gravitational force calculations in an N -particle system. The tree is built in a ‘top-down’ fashion by ‘recursive coordinate bisection’ where on each tree level we split the longest side of a cell through its centre of mass. This procedure continues until the average number of particles in the lowest tree level has dropped below a prescribed value. To calculate the forces on the particles in each lowest-level cell we split the gravitational interaction into a near- and a far-field. Since our main intended applications are SPH simulations, we calculate the near-field by a direct, kernel-smoothed summation, while the far field is evaluated via a Cartesian Taylor expansion up to quadrupole order. Instead of applying the far-field approach for each particle separately, we use another Taylor expansion around the centre of mass of each lowest-level cell to determine the forces at the particle positions. Due to this ‘cell-cell interaction’ the code performance is close to $O(N)$ where N is the number of used particles. We describe in detail various technicalities that ensure a low memory footprint and an efficient cache use.

In a set of benchmark tests we scrutinize our new tree and compare it to the ‘Press tree’ that we have previously made ample use of. At a slightly higher force accuracy than the Press tree, our tree turns out to be substantially faster and increasingly more so for larger particle numbers. For four million particles our tree build is faster by a factor of 25 and the time for neighbour search and gravity is reduced by more than a factor of 6. In single processor tests with up to 10^8 particles we confirm experimentally that the scaling behaviour is close to $O(N)$. The current Fortran 90 code version is OpenMP-parallel and scales excellently with the processor number (=24) of our test machine.

Key words: methods: numerical – methods: N-body simulations – gravitation – hydrodynamics.

1 INTRODUCTION

Self-gravity is a vital ingredient in the simulation of many astrophysical systems. Due to its long-range nature, self-gravity often becomes the major computational burden in simulations of N -body systems or self-gravitating fluids. While many methods exist to calculate gravitational forces under various circumstances (e.g. Hockney & Eastwood 1988), for general self-gravitating systems without particular symmetries hierarchical methods seem to be best suited. The most popular such approaches are tree methods (Barnes & Hut 1986; Press 1986; Hernquist & Katz 1989; Benz et al. 1990; Couchman 1991; Couchman et al. 1995; Dubinski 1996; Stadel 2001; Wadsley et al. 2004; Springel 2005; Nelson, Wetzstein & Naab 2009), and –used to a lesser extent in astrophysics– the fast multipole method (FMM) originally suggested by Greengard & Rokhlin (1987). While tree methods restrict the order of their inherent multipole expansion (usually to quadrupole order) and open up fur-

ther nodes for higher accuracy, the FMM instead fixes an acceptable error measure and then calculates whatever multipole order is necessary to achieve it. According to the common consensus, tree methods are advantageous for problems where a moderate force accuracy can be accepted and where one instead invests available computational resources in larger particle numbers, while the FMM shows its true strength at higher accuracy. There has, however, been recent progress in implementations of error-controlled variants of the FMM (Dachsel 2010) and therefore the above consensus may need to come under renewed scrutiny.

Hybrid methods combining elements of both trees and the FMM have also been developed and successfully tested. For example, Dehnen (2000, 2002) has developed a fast tree method that borrows from the FMM the idea of Taylor-expanding the fields at the ‘sink cells’ in order to calculate the accelerations at individual particle positions. This ‘cell-cell-interaction’ ensures a numerical complexity proportional to $O(N)$ rather than $O(N \log N)$ like standard tree methods (N being the number of particles).

Other Poisson solvers, such as the particle-particle–particle-mesh

^{*} E-mail: e.gafton@jacobs-university.de

(P3M) method, share the same philosophy of approximating forces due to distant particles while computing nearby interactions directly, and exhibit the same $O(N \log N)$ complexity. Although not so widely used by the stellar astrophysics community, P3M codes have been successfully employed in a large variety of cosmological simulations (Efstathiou et al. 1985; Couchman 1991; Macfarland et al. 1998) and also combined with SPH (Evrard 1988). Hybrid methods combining particle-mesh methods with trees, so-called TreePM methods, have also been extensively used in cosmological simulations (Xu 1995; Bode et al. 2000; Bagla 2002; Bagla & Ray 2003; Springel 2005).

Here, we describe in detail our newly developed recursive coordinate bisection (RCB) tree. It will replace an optimized version of the Press tree (Press 1986; Benz, Thielemann & Hills 1989) that we have used for years in our existing codes (Rosswog & Davies 2002; Rosswog & Price 2007; Rosswog et al. 2008). Our new tree will also become a core ingredient of a new SPH code that is currently under development. Since each of these codes has its own peculiarities in terms of input physics, time integration schemes etc., we restrict ourselves in this paper to a self-contained description of our tree module (methods and implementation details) and defer questions such as time integration etc. to a later point. The main purpose of this paper is to document in detail the entity of our tree ingredients and their interplay for future reference. Some of our tree ingredients have also been used in other tree implementations, this will be discussed further in Sec. 2.5.

Our tree is designed to efficiently find neighbour particles for smoothed particle hydrodynamics (SPH) calculations and for the fast calculation of gravitational forces. We were guided by applications which do not exhibit any particular symmetries, such as stellar collisions and tidal disruptions of stars by black holes. In simulations that involve black holes particles are frequently absorbed near the horizon, and therefore just ‘repairing’ an existing tree becomes difficult. Instead, such simulations usually require a frequent and complete re-building of the tree from scratch. Therefore an efficient tree building phase is crucial for our intended purposes. This is part of the reason why we decided for an RCB tree during the code design phase.

Our code has been written from scratch in clean Fortran 90 and does not make use of any external libraries. It is hardware- and platform-independent and as versatile as possible, making no assumptions about the problem type or the particle distribution. It particularly aims at scaling well on a large number of processors (for now using OpenMP) and at being memory efficient. It implements a number of optimization techniques that we describe in detail below. As we will demonstrate, our tree scales close to $O(N)$ for large particle numbers.

The remainder of the paper is structured as follows. In Sec. 2 we describe in detail how we build and walk the tree, and how we use it for efficient neighbour search and gravity calculations. In Sec. 3 we present a set of challenging benchmark tests where we compare our new results against those obtained with the so-called ‘Press tree’ (Press 1986; Benz, Thielemann & Hills 1989) that is widely used in astrophysics (e.g. Benz et al. 1990; Bate, Bonnell & Price 1995; Bonnell, Bate & Vine 2003; Price & Bate 2009; Nelson et al. 2009) and that we have frequently used ourselves (Rosswog et al. 1999; Rosswog & Davies 2002; Rosswog 2005; Price & Rosswog 2006; Rosswog, Ramirez-Ruiz & Hix 2009; Dan et al. 2011). In Sec. 4 we summarize the main features of our tree method.

2 A RECURSIVE COORDINATE BISECTION (RCB) TREE

The underlying idea of a tree method is to collect particles into hierarchically organized groups (sometimes we also refer to them as ‘nodes’ or via their enclosing ‘cells’) so that expensive tasks can be performed on aggregated quantities of the groups rather than on individual particles. For astrophysical purposes, a tree method needs the following ingredients: i) a strategy how to aggregate particles into a hierarchy of groups (‘tree build’), ii) composition formulae to calculate the properties of a ‘mother’ cell from the properties of its ‘daughters’, iii) an ‘opening criterion’ that decides while combing through the tree whether a node can be accepted ‘as is’ or needs to be opened up into its lower level constituents, and finally iv) a prescription how to calculate forces from a list of aggregated nodes.

Particularly popular in astrophysics are the Barnes-Hut octree, henceforth ‘BH tree’ (Barnes & Hut 1986; Hernquist 1987; Turner et al. 1995; Springel 2005; Merlin et al. 2010) and the mutual nearest neighbour binary tree due to Press (Press 1986; Benz et al. 1989).

The method of choice for constructing our tree is ‘recursive coordinate bisection’. Initially all particles are grouped in a root cell and in subsequent steps the longest side of each cell is split through its centre of mass. This leaves an approximate balance between the particle numbers in each of the two resulting daughter cells. The process is repeated until the average particle number per cell has dropped below some pre-defined, empirically-optimised limit, that we will later refer to as \bar{N}_{II} . Our procedure results in a binary tree structure that is extremely fast to build up. Such trees are frequently used in computer science and are often referred to as *kd*-trees (Bentley 1975). To our knowledge they have only been used in astrophysics in the PKDGRAV code (Stadel 2001) which later became the basis of GASOLINE (Wadsley et al. 2004). In the way we build up our tree it delivers an adaptive mesh structure tailored to the particle distribution. The cells’ labels carry information about local proximity so that the tree structure can be naturally and efficiently used to sort particles according to their spatial distribution. Similar techniques such as Peano or Morton space-filling curves are often used in particle methods to improve the computational speed via enhanced cache-coherence.

In the remainder of this section we describe in detail how we build up our tree (Sec. 2.1), how we traverse it (Sec. 2.2) and search for neighbours (Sec. 2.3). The gravity calculations are described in Sec. 2.4 and in Sec. 2.5 we compare our approach with other work.

2.1 Tree build

2.1.1 Strategy

A tree build can either follow a ‘top-down’ strategy where a root node that contains all particles is successively tessellated into smaller entities (‘nodes’ or ‘cells’), or a ‘bottom-up’ approach, where, starting on the level of individual particles groups are formed that are subsequently collected into groups of groups and so on. The BH tree is an example of a top-down tree, the Press tree is a bottom-up tree. Building a tree in a top-down approach is substantially faster (Makino 1990), but it may generate situations in which particles that are well separated in space are artificially placed in the same node, while nearby particles are placed in different nodes. The factors that minimize the chances of this happening are the degree of decomposition and the load balancing algorithm,

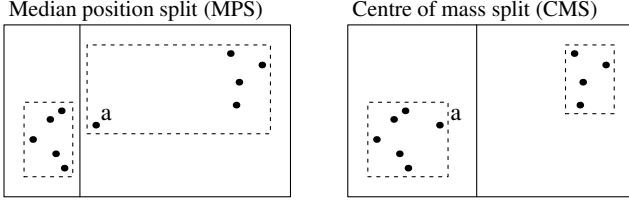


Figure 1. A 2D illustration of two ways to split a given cell: the median position split (MPS, left) and the centre of mass split (CMS, right). The MPS leads to perfectly balanced daughter nodes, but can artificially separate particles that naturally belong to the same group, as illustrated by particle *a*. Since we calculate our gravitational forces by a Taylor expansion around the centre of mass, the MPS can lead to large force errors, therefore we prefer the CMS for building our tree.

which together define the prescription how a node is split into its children.

2.1.2 Degree of decomposition

Octrees (quadrees in 2D) split a cell into eight (four in 2D) daughter cells, binary trees only in two. Therefore octrees are $\frac{\log 8}{\log 2} = 3$ times shorter than binary trees and usually faster to construct. But by forcing all sides to be split, they tend to create elongated daughter cells out of elongated parent cells. This is usually not desirable since such cells can have large high-order multipole moments and can thus introduce large truncation errors in the force calculation. In our binary tree approach we divide a node through its longest edge, which tends to drive daughter cells closer to the desired, compact shape. Binary trees also tend to return shorter interaction lists for a given accuracy (Anderson 1999; Waltz et al. 2002), which reduces the number of direct force evaluations and thus speeds up the gravity calculations.

2.1.3 Load balancing

An important concern is keeping the decomposition of a tree balanced in the sense that sibling nodes contain comparable amounts of particles. Most implementations of the BH tree are *spatially-balanced*, cutting the edge of a cell through its middle. While this method is extremely fast because one only has to compute the average of two coordinates, it can lead to very uneven particle distributions. *Density-balanced* trees, on the other hand, ensure that comparable computational domains remain on each side after the cut. In the design phase of our RCB tree, we have experimented with a median position split (MPS) and a centre of mass split (CMS), see Fig. 1. The MPS produces perfectly balanced particle numbers in each daughter cell, but it can lead to an artificial separation of particles that one would consider as belonging to the same group into different nodes. This is more than just an aesthetic flaw, since due to our Taylor expansion around the cell centre of mass, see Sec. 2.4, particles that are artificially separated from their natural group of peers (e.g. particle *a* in Fig. 1, left) suffer substantially larger truncation errors for the MPS than for the CMS case. In our experiments we found that the relative force accuracy of such ‘renegades’ can be improved by orders of magnitude if the CMS is used instead. Another example would be a stellar binary system containing different numbers of particles per star. The CMS assigns each star its own node, while the MPS would place some of the particles from the heavier star in the node of the lighter star, creating elongated cells and substantially larger multipole truncation errors.

In passing we note that one does not necessarily have to split a cell through its centre of mass, although this is convenient for our applications. If systems with charges of different signs are simulated, say in plasma physics, it may be more convenient to split through the ‘centre of number’ (by simply replacing the particle masses by a weight of ‘1’), and then use the proper charges for the calculation of the needed multipoles.

By choosing the CMS rather than the MPS we pay the price that empty lowest-level cells (‘ll-cells’) can, at least in principle, occur. The CMS procedure will often assign different numbers of particles to sibling cells and therefore one can eventually end up with empty ll-cells at the expense of other ll-cells being over-populated. The latter will be very compact (since high densities are the reason why imbalanced distributions are obtained in the first place), and the multipole expansion will converge. At the same time, empty cells (less than 1% of the total number of cells even for pathological cases) can be safely ignored, since they do not contain neighbours and do not contribute to gravity either.

2.1.4 Particle sorting

One technique that is frequently used in particle methods in order to reduce the number of cache misses is re-ordering the particles in memory based on their physical proximity (e.g. Springel 2005; Thacker & Couchman 2006; Nelson et al. 2009). In experiments of stellar collisions we had found that particle sorting can easily improve overall runtimes by a factor of a few, concluding that the overhead due to sorting is certainly worthwhile the extra effort. The RCB tree uses a customised partitioning algorithm inspired by the quick-sort method (Hoare 1962) to sort the particle arrays.

We first compute the centre of mass of a node, then decide which direction x_i to split, and subsequently perform a single iteration through all the particles in the node. During this iteration, we move all particles that have the x_i coordinate smaller than that of the centre of mass at the beginning of the array, and all particles with larger x_i at the end of the array. The boundary between these two subsets then tells us where the particles of the left child node end and those of the right child node begin. There is no need to sort these two subsets of particles any further because on the next level one might have to split along a different side.

One advantage of sorting the particles is that it eliminates the need to keep a list of all the particles in an ll-cell, the indices of the first and the last particles being sufficient (this actually holds true for any node, since particles are ‘sorted’ on each level). In addition, looping through the particles in any one node requires no jumps through the memory, and hence the array operations (such as the computation of the centre of mass) prove to be extremely cache-efficient.

It is known that typical quicksort implementations have a worst-case complexity of $O(N^2)$ (Press et al. 1992, Sec. 8.2), usually occurring if one repeatedly uses poorly-chosen pivots on already-sorted arrays. In our case, we compute the centre of mass anyway (since we later need it in the gravity calculations) so the pivot element is always optimally chosen. Since on each of the $\log N$ levels we traverse the arrays just once ($O(N)$), the complexity of this subroutine is always $O(N \log N)$. As will be shown below, see Fig. 14, the tree build takes just a small fraction of the CPU-time (less than a percent) in comparison to neighbour search and gravity, and the sorting, in turn, is just a small fraction of the tree build. The investment of time in sorting is completely negligible but speeds up the tree build subroutine substantially. We also gain nearly a factor

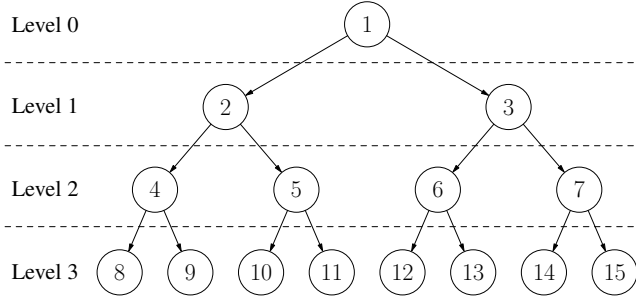


Figure 2. Node labelling convention in the RCB tree. Many useful relations can be trivially recovered by simple arithmetic operations on the node labels without any need for additional memory consumption. See main text for details.

three by substantially enhanced cache access during force evaluations.

2.1.5 Node labelling

A well-chosen node labelling system eliminates the need for pointers that link parent nodes and their children. In the RCB tree, instead of storing the nodes as the components of a linked list (Dubinski 1996; Dehnen 2002; Nelson et al. 2009), we simply use a one-dimensional array, with the relationship between the nodes encoded in their indices.

Our node labelling conventions are illustrated in Fig. 2. For a tree with k levels the total number of nodes is $2^k - 1$. The best choice is to assign the root node the label ‘1’, place it on level ‘0’, and then continue to increment the labels level-by-level. With this labelling convention, simple ‘index gymnastics’ allows to recover various node relations without additional memory consumption. For example:

- (1) the children of node n are $2n$ and $2n + 1$;
- (2) the level of cell n is $\lceil \log_2 n \rceil$ (Gauß bracket);
- (3) the first node on level k is 2^k ;
- (4) the last node on level k is $2^{k+1} - 1$;
- (5) the number of cells on level k is 2^k ;
- (6) the total number of descendants of a cell on level k is $2^p - 2$,

where p is the number of levels greater than or equal to k .

The last relation is used, for example, when entire branches are discarded during the tree walk. Fig. 3 illustrates how the node labels relate to the spatial tessellation for a two-dimensional particle distribution.

2.1.6 Multipole moments

During the tree building phase, a number of physical quantities are calculated and stored for each node: position of the lowest-left corner, size, coordinates of the geometrical centre and of the centre of mass, and the multipole moments. For the gravitational forces from distant nodes we use a simple Cartesian multipole expansion up to quadrupole order. Since the dipole moment vanishes when the origin of the multipole expansion coincides with the centre of mass, one only needs to store the monopole and the quadrupole moments. The monopole is simply the mass of all the particles in the cell and can be computed very fast with the SUM command, since all particles of a given node, having been sorted, are contiguous in memory. For the ll-cells one computes the components of the traceless quadrupole tensor due to each individual particle a ,

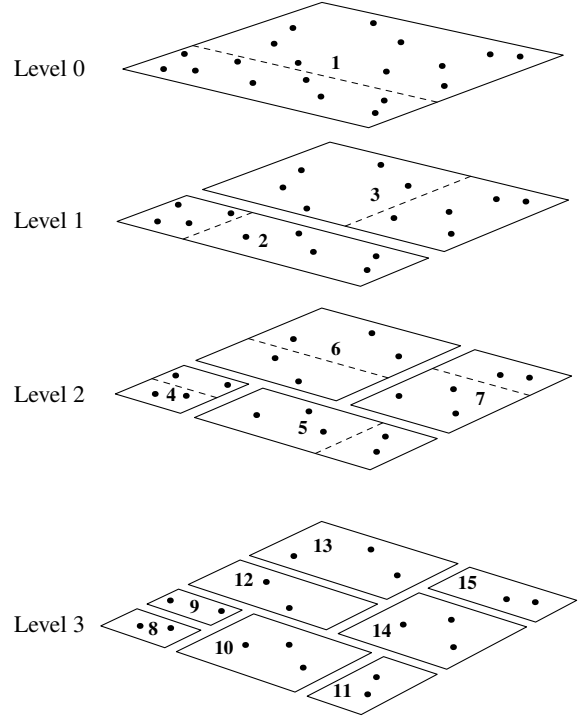


Figure 3. Illustration of the spatial splitting and labelling of cells on different levels for a two-dimensional particle distribution. Dashed lines (planes in 3D) are perpendicular to the longest cell side and cross the centres of mass. The tessellation ends once the average number of particles per lowest-level cell has dropped below a prescribed value, \bar{N}_{ll} .

$$Q_{ij}^a = 3m^a \Delta x_i^a \Delta x_j^a - m^a (\Delta r^a)^2 \delta_{ij}, \quad (1)$$

where m_a is the particle mass, Δx_k^a are the components of the particle a ’s offset from the cell centre of mass and $(\Delta r^a)^2 = \sum_i (\Delta x_i^a)^2$. Subsequently, these quadrupole moments are ‘shifted up’ to the parent nodes. Specifically, the quadrupole moments Q_{ij}^P of a parent node P are computed in terms of the quadrupole moments Q_{ij}^C of its children C as:

$$Q_{ij}^P = \sum_C \left[Q_{ij}^C + 3M^C \Delta x_i^C \Delta x_j^C - M^C (\Delta r^C)^2 \delta_{ij} \right], \quad (2)$$

where M^C is the mass of child C , Δx_i^C is the distance between the centres of mass of the parent and of its child along the axis x_i , and Δr^C is the distance between their centres of mass: $(\Delta r^C)^2 = \sum_i (\Delta x_i^C)^2$.

2.1.7 Parallelisation

Since each level of the tree depends on the previous levels (the particles must be sorted in the parent node before the children nodes can be created) simple OpenMP work sharing constructs will not work out of the box. Instead, we use an MPI-like approach: assuming that 2^k processors are to be used for the tree build, one builds the tree down to level k on just one processor, and then ‘distributes’ each of the 2^k nodes on level k to one processor. Since the particles are sorted down to level k , each processor can now build its own ‘sub-tree’ by simply ignoring the rest of the tree and acting as if its assigned node were the root node.

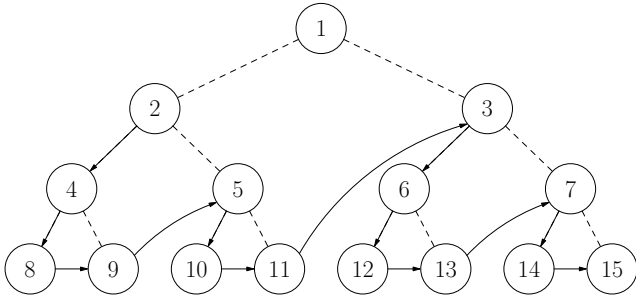


Figure 4. The order in which tree nodes are accessed during a tree walk. Jumps between non-neighbouring cells are indicated by curved arrows. Note that the original connection between a parent cell and its right daughter, marked with dashed lines, is no longer significant for the tree walk. All tree walks begin with node 2.

2.1.8 Updating the tree

Although heavily optimised and never taking more than 1% of the total computational time, the tree build is still an expensive operation that should be avoided when possible. For this reason, the integrity of the tree is checked after every time step: if the particles have not moved out of their ll-cells then the tree does not need to be rebuilt. It is sufficient to simply update the relevant quantities of the ll-cells (centre of mass, radii of influence and quadrupole moments), and then compute these quantities for all the larger cells in a bottom-up manner. Since no tessellation and sorting are required, the procedure is much faster than a full-scale tree build and can be used until one particle crosses the border of its ll-cell. At that point, the tree could in principle be ‘repaired’ by locally adjusting the tree structure where necessary. For now, however, we completely rebuild the tree whenever this ‘integrity check’ fails, otherwise we just update it.

2.2 Tree walk

In order to find properties (such as neighbours or gravitational forces) of particles in the ll-cells we have to ‘walk the tree’. Recursive tree walks can be programmed elegantly and in a very compact way, but they are usually too inefficient for use in astrophysical applications, since they complicate to take optimization decisions at compile time and each recursive call comes with its own computational overhead. We have implemented a modified version of the depth-first search algorithm (Cormen et al. 2001, §22.3) which has been used in astrophysical applications, for example, by Dubinski (1996). The order in which the tree nodes are accessed is shown in Fig. 4.

A tree walk requires a criterion (one for a neighbour and one for a gravity walk) for the decision whether to accept a node or to open it and examine the two daughter nodes. If an ll-cell cannot be accepted then all its particles are processed individually. A tree walk ends when all the nodes in the tree have been either opened or skipped. Since the root node contains all the particles, it can never be accepted by any criterion; hence, the tree walk always begins with node 2.

2.2.1 Tree vector

The tree needs to be walked at least once per time step for every ll-cell that needs an update, therefore the tree walk efficiency is of key importance for the overall runtime. The computations involved

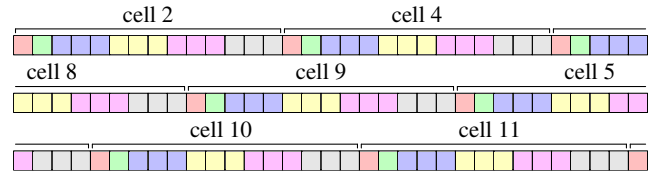


Figure 5. The ‘tree vector’ is a one-dimensional array which stores all the relevant properties of all nodes contiguously, in exactly the order in which they are accessed during the tree walk, see Fig. 4. This allows for a very cache-efficient data access. In a typical simulation with a few million particles, the use of the tree vector can reduce the time spent for tree walks by as much as two orders of magnitude.

in the neighbour search (simple comparisons) are not complicated, but the sheer memory span that the algorithm has to traverse (a tree can have millions of cells scattered throughout the RAM) can slow down the subroutine considerably. Therefore just accessing the node data in the order of the tree walk would lead to continuous and repeated cache misses for every tree walk and therefore would cause a serious slowdown. The tree data, however, is always accessed in the same order. This led us to the idea of introducing a ‘tree vector’, a one-dimensional array which stores all the needed data (label, level, centre of mass, geometrical centre, position, size) of the nodes contiguously, in exactly the order in which they are accessed during the tree walk. This is illustrated in Fig. 5. The tree vector is created once per time step, directly after the tree build, and it is subsequently used in all the tree walks. Inefficient data access therefore just occurs once (in the tree vector creating stage) rather than hundreds of thousand times during repeated tree walks. The subsequent tree walks all receive their data as a contiguous batch of elements from the tree vector. If a node has to be opened, the next batch of elements, corresponding to the node’s left daughter, is read from the tree vector, and the code simply advances a counter; usually, chances are that this batch is already loaded in cache (since whole segments, and not individual numbers, are read from the RAM at once). If the cell has to be skipped then all its $2^p - 2$ descendants, see Sec. 2.1.5, are skipped, in which case the tree vector counter is simply incremented by the required amount. The tree walk ends when the counter reaches the end of the tree vector. In our benchmark tests with a few million particles distributed according to a Sobol sequence, see Sec. 3, the use of a tree vector speeds up the tree walks by as much as two orders of magnitude.

2.3 Neighbour search

In SPH, continuous or ‘smoothed’ quantities at a given position are obtained by summing up the kernel-weighted properties of contributing particles. Similarly, gradients of fluid properties are calculated as sums over the analytically known kernel gradients (see, e.g., Rosswog (2009) for a recent review of the SPH method). We use here the ‘standard’ cubic spline kernel of Monaghan & Lattanzio (1985), which has compact support and vanishes outside of a finite radius $2h$. Since contributing particles (‘neighbours’) need to be known at every time step, it is crucial to have a very efficient algorithm to identify them.

2.3.1 Neighbour walk

To determine possible neighbour candidates, we walk the tree as described above for every ll-cell that requires an update. During the tree walk we check whether a candidate cell B can be reached

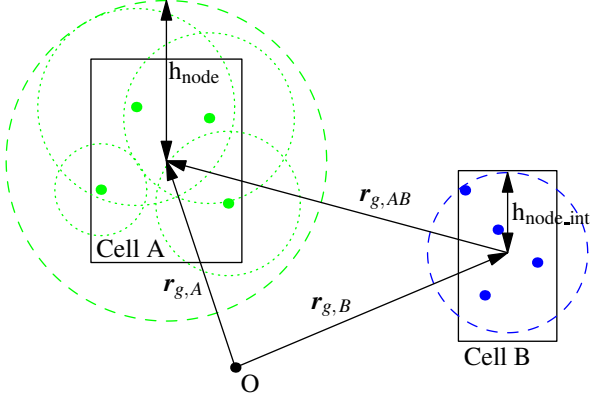


Figure 6. The radius h_{node} of cell A (dashed green circle) encompasses the kernels of all the particles in A (dotted green circles). The interaction radius $h_{\text{node,int}}$ of cell B (dashed blue circle) encompasses all particles in B. If we denote the distance vector between the geometric centres of the cells by $\mathbf{r}_{g,AB} = \mathbf{r}_{g,A} - \mathbf{r}_{g,B}$, the ‘reachability condition’ translates into $|\mathbf{r}_{g,AB}| < h_{\text{node}}(A) + h_{\text{node,int}}(B)$. If this test fails, cell B is discarded and all its children are skipped in the tree walk.

from the cell of interest, cell A. To this end we had assigned in the tree building phase to each ll-cell the ‘interaction radius’ $h_{\text{node}}(A)$, which encloses the volume covered by the individual kernels of all its particles, see Fig. 6. Moreover, each cell B had been assigned a radius $h_{\text{node,int}}(B)$ that starting from the geometric centre of cell B enclosed all its particles. The particle content of cell B is included in a ‘candidate list’ for possible neighbours of particles in cell A, if

$$|\mathbf{r}_{g,AB}| \equiv |\mathbf{r}_{g,A} - \mathbf{r}_{g,B}| < h_{\text{node}}(A) + h_{\text{node,int}}(B), \quad (3)$$

i.e. if particles in cell A can possibly reach at least one of the particles in cell B. Although not strictly necessary, in a subsequent step we cull the candidate list to the true neighbours to save some computational effort during the later summation stage (to calculate densities and the hydrodynamic derivatives).

2.3.2 Neighbour list

Storing a list of neighbours for each particle can be problematic: we typically use a neighbour number of ~ 100 per particle (Rosswog 2009, Sec. 2.9), but under certain circumstances individual particles can have a much larger number of neighbours. This can happen, for example, if low-density regions with large smoothing lengths interact with high-density regions with small smoothing lengths. If a low density particle is expanding, even a small fractional increase of its smoothing length can lead to a large jump in the neighbour number if suddenly the high density region ‘becomes visible’. Under such circumstances one has two possibilities: either fine-tune the smoothing length immediately to a value so that the neighbour number is in an acceptable range, which can introduce a substantial amount of numerical noise, or accept the large neighbour number for a few time steps for this particle, in which case one has to take care of the storage of a very long neighbour list for the respective particle. Since such situations are exceptions, it is a waste of memory to store ‘worst-case-sized’ lists of neighbours in a fixed bi-dimensional array (such that neighbours $1 \dots k$ of particle n are stored at positions $(n, 1 : k)$); one would have to allocate the maximum space for each particle, even though most of them will have far fewer neighbours.

An elegant solution to this problem is to store the neighbours in

a one-dimensional list. This comes with a slight computational overhead, since one has to also store, for each particle, the total number of neighbours and the index of its first neighbour in the one-dimensional list. The memory savings, on the other hand, are tremendous, for one has to only allocate an ‘average’ number of neighbours per particle, rather than a ‘maximum’ one.

2.3.3 Parallelisation

If the ll-cells whose neighbours have to be updated are distributed to different processors, the computations are independent and can be programmed with OpenMP work-sharing constructs. We use dynamical scheduling – gradual allocation of the iterations to various threads as they become idle – in order to prevent load imbalance. Combining the results in a one-dimensional array, however, constitutes a possible bottleneck, since different threads might want to simultaneously modify the same array, in which case they are queued in the order in which they finish their calculations. This introduces a waiting time of a few percent of the total neighbour search, but is nevertheless preferable to using a bi-dimensional array.

2.4 Gravitational forces

To achieve accurate gravitational forces at a moderate computational effort, we split gravity into a near- and a far-field contribution. The near-field component is crucial for the accuracy and it is obtained by a kernel-smoothed direct summation, while the far-field contribution is calculated via a low-order multipole expansion up to quadrupole order. The gravitational constant G is set to unity throughout the paper.

2.4.1 Multipole acceptance criterion

During a gravity tree walk a multipole acceptance criterion (MAC) decides whether a node can be accepted with its multipole moments or whether it needs to be further resolved into its constituents for higher accuracy. In the first case all descendants can be skipped, in the second case the tree walk advances down the tree until either the acceptance criterion is met, or a lowest-level cell is reached, in which case all its particles are added to a near-field list. After experiments with various criteria that have been published in the literature (Salmon & Warren 1994; Nelson et al. 2009) we decided for the simple geometric MAC introduced by Barnes & Hut (1986): a cell B is accepted if the opening angle under which it is seen drops below a prescribed accuracy parameter θ :

$$\frac{H_B}{R_{AB}} < \theta \quad \text{with} \quad H_B = \text{MAX}(S_{i,B}). \quad (4)$$

Here, the $S_{i,B}$ are the side lengths of cell B and $R_{AB} = |\mathbf{r}_A - \mathbf{r}_B|$ is the distance between the centres of mass of cells A and B. For $\theta = 0$ this reproduces, of course, the direct summation case. Furthermore, if a cell B contains potential neighbour particles, we add its constituents to the near-field list, and do not accept the cell, independent of the MAC. This leads to relatively long near-field lists (~ 800 particles), which come at an N^2 -price, but which are also important for high force accuracy. Moreover, the near-field contribution parallelizes perfectly well, so for large parallel calculations this becomes an acceptable procedure. As we will show below, our algorithm is very efficient despite the relatively long near-field lists. The rare, potentially unbounded errors introduced by the simple geometric MAC and described by Salmon & Warren (1994) are avoided in our code, as explained in Sec. 3.1.

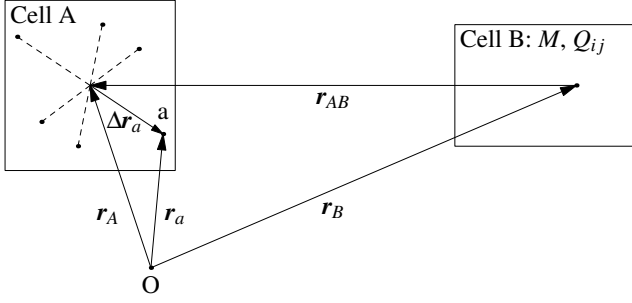


Figure 7. Forces at particle positions are calculated via a Taylor expansion around the cell centres of mass. For a particle a at position \mathbf{r}_a , the acceleration \mathbf{f}_a due to cell B is obtained by Taylor expanding $\mathbf{f}(\mathbf{r}_A + \Delta\mathbf{r}_a)$ around \mathbf{r}_A .

2.4.2 Far field

The multipole expansion of the gravitational potential $\Phi(\mathbf{r})$ due to a distant node with mass M and quadrupole moments Q_{ij} reads in Cartesian coordinates:

$$\Phi(\mathbf{r}) = -\frac{M}{r} - \frac{1}{2} \sum_{i,j} \frac{x_i x_j}{r^5} Q_{ij} + O(r^{-7}). \quad (5)$$

Once a list of acceptable, distant nodes has been identified via a tree walk, the resulting accelerations can be calculated as the gradients of the truncated potential, $\mathbf{f}(\mathbf{r}) = -\nabla\Phi(\mathbf{r})$. We calculate the far gravity acceleration on particles in a given ll-cell via ‘cell-cell interaction’, similar to what is done in the FMM and the tree code of Dehnen (2000, 2002). To this end we calculate the Taylor expansion of the forces around the centre of mass of an ll-cell, see Fig. 7. For a particle a in cell A the far-gravity contribution reads to second-order:

$$\mathbf{f}_{\text{fg}}(\mathbf{r}_a) = \mathbf{f}_{\text{fg}}(\mathbf{r}_A + \Delta\mathbf{r}_a) \simeq \mathbf{f}_{\text{fg}}(\mathbf{r}_A) + \mathbf{J}_A \Delta\mathbf{r}_a + \frac{1}{2} \Delta\mathbf{r}_a^T \mathbf{H}_A \Delta\mathbf{r}_a. \quad (6)$$

Here, \mathbf{J}_A and \mathbf{H}_A are the Jacobian and Hessian as evaluated at point \mathbf{r}_A . In three dimensions they only have 6 and 10 independent components, respectively, due to the equality of mixed partial derivatives. This Taylor expansion allows to evaluate the far gravity only once per ll-cell and ensures the approximate $O(N)$ behaviour for large N .

2.4.3 Near field

Our goal is to simulate a self-gravitating fluid rather than a point particle system. Therefore, the mutual interaction between nearby particles needs to be softened. We use the SPH kernel function W to smooth both hydrodynamics and near-field gravity in a consistent way. The kernel-softened force (e.g. Dyer & Ip 1993; Dehnen 2001) on a particle a due to b is given by:

$$\mathbf{F}_a = -\frac{m_a m_b}{r_{ab}^2} \eta_{ab} \hat{\mathbf{e}}_{ab}, \quad (7)$$

where the softening is mediated via

$$\eta_{ab} = 4\pi \int_0^{r_{ab}} r^2 W(r, h) dr. \quad (8)$$

Here we have used $\hat{\mathbf{e}}_{ab} = \mathbf{r}_{ab}/r_{ab}$, $\mathbf{r}_{ab} = \mathbf{r}_a - \mathbf{r}_b$. Thus the gravitational force is smoothly switched off as the particles approach each other. For constant h , Poisson’s equation shows that this force law corresponds to the force on a point particle a due to a density $\rho(\mathbf{r}_a) = m_b W(r_{ab}, h)$. For the commonly used cubic spline kernel

(Monaghan & Lattanzio 1985) the near gravity acceleration on particle a then becomes

$$\mathbf{f}_{\text{ng}}(\mathbf{r}_a) = -\sum_{b \neq a} m_b S(r_{ab}, h) \hat{\mathbf{e}}_{ab} \quad (9)$$

with

$$S(q) = \begin{cases} 1/h^2 \left(\frac{4}{3}q - \frac{6}{5}q^3 + \frac{1}{2}q^4 \right), & 0 \leq q < 1 \\ 1/h^2 \left(\frac{8}{3}q - 3q^2 + \frac{6}{5}q^3 - \frac{1}{6}q^4 - \frac{1}{15q^2} \right), & 1 \leq q < 2 \\ 1/r^2, & q \geq 2 \end{cases} \quad (10)$$

and $q = r_{ab}/h$. To ensure exact conservation, S should be symmetric with respect to the particle labels a and b , which we enforce by using $h = 0.5(h_a + h_b)$.

Alternatively, a discretized set of self-gravitating SPH equations can be derived consistently via a variational principle from a Lagrangian which contains an ideal fluid contribution and additional self-gravity terms (Price & Monaghan 2007). Such an approach delivers consistently softened SPH equations and in addition also ‘gravitational grad- h ’ terms which are similar to the correction terms derived for the SPH equations (Springel & Hernquist 2002; Monaghan 2002). Such a treatment is beyond our current focus, but if desired, it can be implemented in a straight forward way.

2.4.4 Parallelisation

Since computing the gravitational accelerations acting on two different ll-cells involves unrelated calculations, dynamically scheduled OpenMP work-sharing constructs work well for the gravity calculations and no specific optimisation is needed.

2.5 Comparison with other work

Some elements of our RCB tree have been used in previous work. Here we will briefly summarize similarities and differences. The most commonly used type of tree in astrophysics is the Barnes-Hut oct-tree. Since we have outlined some basics above and since this type of tree is fundamentally different from ours, we do not further discuss it here.

The only astrophysical tree that is built similar to ours (as a kd-tree), is the one used in GASOLINE (Wadsley et al. 2004) which is based on the PKDGRAV code (Stadel 2001). It also does not build the tree down to the particle level, but instead down to what the authors call ‘buckets’, which correspond to our ll-cells. There are a number of differences between GASOLINE and our tree. In GASOLINE cells are split according to MPS while we use CMS, see Sec. 2.1.3. We found the CMS splitting to be substantially more accurate in terms of worst case errors. The authors calculate far-gravity contributions *per particle* using a hexadecupole expansion for acceptable cells while we calculate it *per ll-cell* using a quadrupole expansion and obtain the forces at particle positions via a Taylor expansion. Also the near-gravity approach differs. They base their direct summation list decision on a purely cell property-based opening criterion, their Eq. (1), which does *not* involve any information about the smoothing lengths. Therefore, no consistency between hydrodynamics and gravity is guaranteed in the sense that hydrodynamically interacting particles also interact (i.e. are smoothed) gravitationally. In principle, this can deteriorate the conservation properties, but depending on the chosen parameters this may or may not be relevant in practical simulations. We pursue a more conservative (though somewhat more costly) strategy in the sense that reachable cells are added to the direct summation list, independently of the MAC. However,

if further optimization is desired, this could be changed by simply modifying one line in the gravity-walk subroutine.

As will be shown below, our tree scales close $O(N)$, which is due to the far-force being calculated via a Taylor expansion only once per ll-cell. Such cell-cell interactions are at the heart of the FMM method (Greengard & Rokhlin 1987). The idea of cell-cell interactions, i.e. using Taylor expansions at both the ‘sink’ and the ‘source’ side, has been used in the $O(N)$ tree of Dehnen (Dehnen 2000, 2002). Contrary to our approach, Dehnen uses a standard oct-tree structure and makes explicit use of symmetries in the double-sided Taylor expansions in order to reduce the operational effort. Combined with a MAC that is symmetric in the properties of the two interacting cells this explicitly enforces momentum conservation by ensuring that Newton’s third law is obeyed. The benefits of this approach come at the price of larger memory consumption; also, the explicit use of the symmetries in Taylor expansion coefficients (cells are evaluated as both ‘sinks’ and ‘sources’) prevents the use of standard tree walks. Instead, Dehnen uses a two step approach with an ‘interaction’ and ‘evaluation’ phase, see Sec. 3.2 in Dehnen (2002) for details. The benefit of exact conservation, however, needs to be given up when individual time steps are used.

Moreover, Dehnen’s tree is designed for N-body codes rather than for simulating self-gravitating fluids as in our case. Therefore, the MAC is not ‘overruled’ by a ‘reachability’ criterion as in our (conservative) approach described in Sec. 2.4.1. As an effect, the near-field lists can be kept shorter which reduces the cost of the direct summation part of the code. As outlined above, such an approach could be easily implemented in our tree, but for now we stick to the more conservative (and slightly more expensive) approach.

3 BENCHMARK RESULTS

Motivated by possible future applications of our RCB tree code, we chose three sets of initial conditions: particles distributed in a sphere according to a quasi-random Sobol distribution (Press et al. 1992), see Fig. 8, and two snapshots from SPH simulations: a white dwarf – white dwarf (WD–WD) collision with 602506 particles (Rosswog et al. 2009), see Fig. 9, and a WD (500677 particles) that has been tidally disrupted by an intermediate-mass black hole (IMBH) of $1000 M_\odot$ (Rosswog et al. 2009), see Fig. 10. The Sobol sequence yields particles that homogeneously fill the allowed space (here a sphere), but its quasi-randomness makes it a ‘worst case scenario’ for efficient memory access. The other two scenarios are close to the future applications of our code and they are challenging in terms of a complicated geometry with a very large spectrum of particle densities and smoothing lengths and in the sense that the particles are scattered across memory, i.e. spatially nearby particles are *not* close in terms of memory location.

As explained above, our tree will become an ingredient of several codes which will differ in their time integration methods. Therefore, we only present tests of speed and force accuracy calculations for static particle distribution snapshots. We aim for an average relative force error of $\approx 0.1\%$, but also monitor the force errors of all particles to make sure that even the most extreme outliers remain at an acceptable accuracy. This is crucial since among our intended applications are neutron stars which, as a result of their nearly incompressible matter equation of state at high density, exhibit very sharp surfaces. Particles with large errors in such a surface region can be disastrous for the whole simulation.

For all tests we compiled the serial code with the Intel Fortran 9.1 compiler, using the `-O3` optimisation flag and the double precision

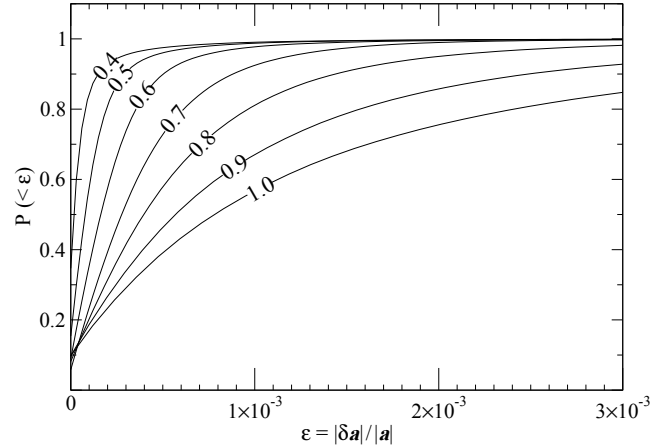


Figure 11. Cumulative error curves for $\theta = 0.4, 0.5, 0.6, 0.7, 0.8, 0.9$ and 1.0 , showing the fraction $P(< \epsilon)$ of particles with relative errors $|\delta \mathbf{a}_i|/|\mathbf{a}_i|$ smaller than the value ϵ given on the x axis. This figure has been obtained for the particle distribution of a WD–WD encounter ($N = 602506$, $\theta = 0.7$). All other cases yield very similar distributions.

flag `-real-size 64`. The code was executed on an Intel Xeon E5420 processor running at 2.50 GHz, with 6 MB of L2 cache and 8 GB of RAM.

3.1 Accuracy

As a first test we explored the sensitivity of the force accuracy to the parameter θ . The cumulative distribution of relative errors in the acceleration, $\epsilon_i = |\delta \mathbf{a}_i|/|\mathbf{a}_i|$, was investigated for θ in a range from 0.4 to 1. Our RCB tree results are compared against direct, kernel-smoothed summations according to Eq. (9) which are correct to double precision accuracy (15 significant digits). The cumulative error distributions are plotted in Fig. 11. For $\theta = 0.7$, 99% of the particles have relative errors less than 0.2%. Fig. 12 shows in detail the relation between the relative force errors ϵ_i and the absolute values of the force, $|\mathbf{a}_i|$, in a typical simulation. Since the plots for our test cases are quantitatively very similar, we only present the results for the WD–WD encounter. Also, since the particles with $\epsilon < 0.2\%$ are uniformly distributed across the entire force spectrum, we do not plot them. The plot demonstrates that all the particles with large relative errors only experience a very weak total gravitational force.

The above accuracy is acceptable for most astrophysical applications, therefore we make $\theta = 0.7$ our default value. We find that the accuracy plots for all three particle distributions are virtually identical, therefore we display only the results for the WD–WD encounter. This robustness with respect to the geometry of the particle distribution underlines the versatility of our approach and is a highly desired property for an astrophysical simulation algorithm. In all of the cases, the very few particles with relative errors above 0.2% feel an essentially zero net force. Formally, of course, this relative error can diverge (for exactly $|\mathbf{a}_i| = 0$), but in practice this does not have any influence since the particles just do not move during a time step.

Salmon & Warren (1994) showed that the conventional geometric MAC, see Eq. (4), can introduce unbounded errors in certain pathological cases (see their Appendix A for the ‘detonating galaxies’ scenario). In our RCB tree, these situations are avoided in two ways. On the one hand, the CMS described in Sec. 2.1 protects against having very distant particles in the same cell. On the other

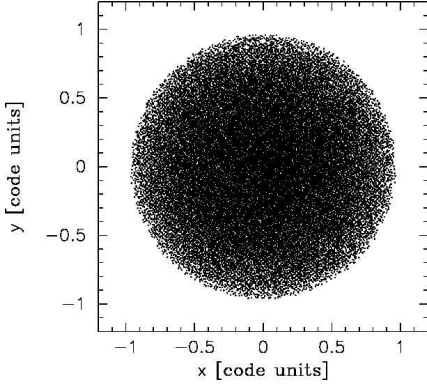


Figure 8. A particle distribution within a sphere, obtained via a Sobol quasi-random sequence. Such a particle distribution is homogeneous, but –due to its randomness– represents a ‘worst case scenario’ for efficient memory access.

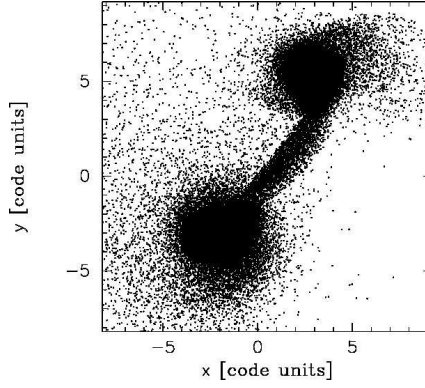


Figure 9. Snapshot from a white dwarf – white dwarf off-centre collision (602506 particles). The smoothing lengths span a range of over three orders of magnitude, due to the large density discrepancy between the stellar centers and the accretion flow between them.

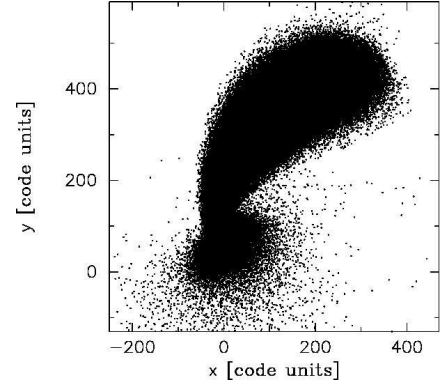


Figure 10. Snapshot from a tidal disruption of a white dwarf (500677 particles) by an intermediate-mass black hole of 1000 M_{\odot} . The large range of smoothing lengths, five orders of magnitude, make the force calculation challenging.

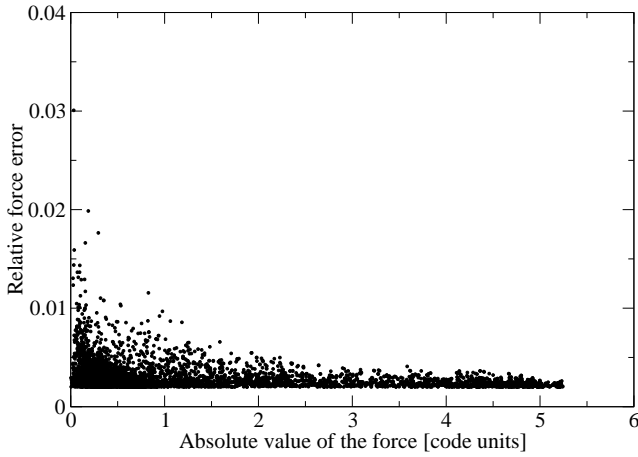


Figure 12. The relative error $\epsilon = |\delta a|/|a|$ plotted against the absolute value of the force, $|a|$. Accuracies of $\epsilon < 0.2\%$ are obtained for particles across the full force spectrum (for over 99% of all particles). These particles are *not* shown here, instead, we focus in this plot on the outliers. Only particles with very small forces exhibit force errors in excess of 1%. This figure has been obtained for the particle distribution of a WD–WD encounter ($N = 602506$, $\theta = 0.7$). All other cases yield very similar distributions.

hand, since the particle content of each reachable cell is summed up directly and independent of the MAC, we are protected against potentially unbounded errors from particles that get very close to the sink but whose cells are, for some reason, still accepted by the MAC.

3.2 Performance

3.2.1 Optimizing the tree depth

We experimentally optimize the depth of our RCB tree, which is determined by the average number of particles per II-cell, \bar{N}_{II} . Sample results for a spherical Sobol distribution with $N = 500000$ are presented in Table 1. As expected, the tree build becomes faster as the height of the tree decreases, but in none of the cases the tree build takes more than 1% of the total computing time. The neighbour search and the gravity calculations depend strongly on the height

Table 1. Scaling of the RCB tree with the average number of particles per II-cell, \bar{N}_{II} . The following abbreviations are used: L: number of tree levels; $P_{<1\%}$: fraction of particles with an error smaller than 1 %; TB: tree build, N: neighbour search, NG: near-field gravity, FG: far-field gravity, G: total gravity. Times are measured in seconds.

\bar{N}_{II}	L	$P_{<1\%}$	TB [s]	N [s]	NG [s]	FG [s]	G [s]
1	19	0.9998	0.76	23.54	6.14	99.26	171.47
3	18	0.9998	0.51	10.90	7.15	39.76	75.52
6	17	0.9998	0.36	6.67	10.16	16.12	37.83
12	16	0.9998	0.29	5.86	14.66	6.66	25.90
24	15	0.9997	0.25	7.07	22.02	2.71	26.67
48	14	0.9997	0.24	10.56	36.22	1.02	38.13
64	13	0.9996	0.22	14.97	56.90	0.50	57.88
128	12	0.9997	0.19	26.12	101.51	0.18	102.04

The test was performed on a spherical Sobol distribution with 500 000 particles and smoothing lengths chosen so that the average number of neighbours was 105. With our standard value for the accuracy parameter, $\theta = 0.7$, the average relative error $\bar{\epsilon} \approx 0.1\%$ for all test cases. Particles with errors larger than 1% are essentially force free (their force is about five orders of magnitude smaller than the average force). In an extensive set of tests we always found optimal results for $\bar{N}_{II} \approx 12$, regardless of the number of particles or their distribution.

of the tree: larger II-cells mean a shallower tree and thus faster tree walks and far-gravity, while the near-gravity neighbour candidate lists become longer and increasingly more expensive to evaluate. The balance between the two regimes was empirically found at $\bar{N}_{II} \approx 12$ regardless of the number of particles or the complexity of their spatial distribution. The performance is rather robust against substantial changes in this number, e.g. doubling this value to 24 yields essentially the same performance. All of our subsequent test calculations were obtained with $\bar{N}_{II} = 12$.

3.2.2 Comparison with the Press tree

We chose to compare the RCB tree with a commonly used binary tree that is due to Press (Press 1986; Benz et al. 1989), mainly because we have used this tree for years and because this is the tree that our new RCB tree will replace. The version used in this comparison has been tuned by collecting quantities that are

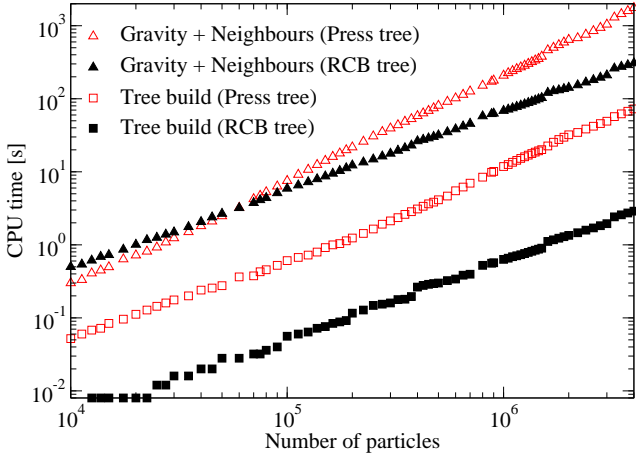


Figure 13. Comparison between the Press and the RCB tree in terms of the tree building time and of the cumulative time required for neighbour search and gravity calculations. The particle distributions for this test were spherical Sobol distributions with up to 4 million particles. The smoothing lengths were chosen such that the average neighbour number was 105. The plot shows a cross-over point for the gravity + neighbours timings at $N \approx 50000$: for very low particle numbers, the complex infrastructure of the RCB tree renders it slower (up to a factor of two) than the Press tree.

frequently used together into common arrays (Rosswog & Price 2007). This has improved the overall performance for completely unsorted particle arrays by nearly a factor of three with respect to the original version. We have chosen the accuracy parameters of the two trees so that we obtain overall very similar accuracies, an average relative error of $\bar{\epsilon} \approx 0.1\%$ and a maximum error $\epsilon_{\max} \lesssim 1\%$, but with the RCB tree being slightly more restrictive and producing slightly higher accuracies. This motivated our choice of $\theta_{\text{Press}} = 0.5$ for the Press and $\theta_{\text{RCB}} = 0.7$ for our RCB tree. The larger θ -value for the RCB tree has two explanations: the Press tree has tight bounds by construction (Anderson 1993) and thus exhibits physically smaller nodes, and the MAC in our RCB tree is more conservative in the sense that it chooses the longest cell edge as a measure of the cell size, see Eq. (4).

Tree build

In a first test we compare the performance during the tree building phase. Due to the more complicated algorithm for identifying mutual nearest neighbours, building the Press tree from scratch is quite time consuming. In fact, from all the trees frequently used in astrophysics, the Press tree is probably the most expensive one to build. As test cases we chose spherical Sobol distributions with smoothing lengths so that the average neighbour number was 105 (this is conservative for the gravity calculation with our RCB tree algorithm since it uses large particle numbers in the direct, near-gravity summation and the results would be even stronger in favour of the RCB tree for smaller neighbour numbers). The results of this test are presented in Fig. 13 with filled (open) squares for the RCB (Press) tree. Here, the RCB tree turns out to be substantially faster than the Press tree, for 4×10^6 particles (the maximum we could afford for our version of the Press tree) on one processor our RCB tree build is already ~ 25 times faster than the Press tree with increasing discrepancy for larger particle numbers.

Neighbour search and gravity

The second performance measure is the sum of the times for neighbour search and gravity. The reason for summing them up is that

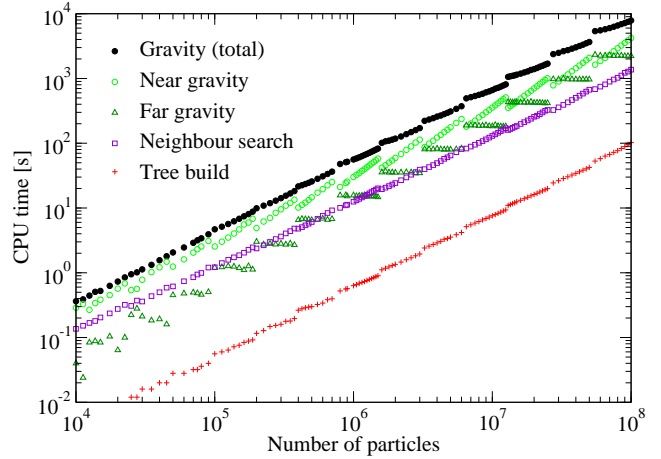


Figure 14. Comparative timings of the RCB tree code components (tree build, neighbour search and gravity calculations) for spherical Sobol distributions with up to 10^8 particles and ~ 105 neighbours per particle. Since the far-field gravity calculation does not depend on the particle number, but only on the tree depth the ‘far gravity’ in the plot remains essentially constant until the number of tree levels is incremented. The tree build always takes less than 1% of the execution time, the gravity calculation typically takes 80-90% percent, and the neighbour search occupies the remaining 10-20%.

our version of the Press tree performs both operations in the same loop for increased performance. We decided to keep the RCB tree code flexible and separate the two operations in different subroutines that can be called independently. One would therefore expect the RCB code to perform even better if one was willing to sacrifice this flexibility and to calculate both in a single loop. The RCB tree outperforms the Press tree in this test already at $N \approx 50000$, see the filled triangles for the RCB and the open triangles for the Press tree. Up to this point its relatively complex infrastructure makes the RCB tree slower (up to a factor of two, for these particle numbers corresponding to fractions of a second on one processor). Near 4×10^6 particles, however, RCB neighbour search and gravity are faster by about a factor of 6 with larger discrepancies for increasing particle numbers. In this and the subsequent plot one notices little ‘glitches’ in the RCB curves. They occur whenever the height of the tree changes, since tree walks and far-field calculations, being performed ‘per ll-cell’ rather than ‘per particle’, only depend on the number of ll-cells and not directly on the number of particles.

3.2.3 Behaviour for large N

In order to test the robustness and the scaling behaviour of our RCB tree we computed, on one processor, the self-gravity of Sobol distributions with increasingly larger particle numbers, ending only at 10^8 particles. Successfully running such a simulation on a machine with only 8 GB of RAM gives an upper limit on the memory consumption of our code of approximately 86 bytes per particle. This includes not only the arrays that store particle properties, but also the ones that store the nodes, the temporary variables, the subroutines, the files read in memory, and every other bit of RAM that our code uses.

In Fig. 14 we compare the time spent for different operations. The tree build becomes completely negligible as the number of particles increases (even in the worst case it never surpasses 1% of the total execution time). The tree build in the Press tree has been one of the most expensive components, see also Nelson et al. (2009),

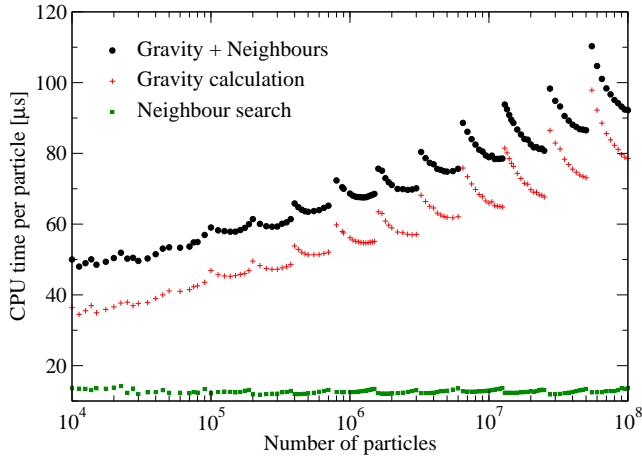


Figure 15. CPU time spent per particle in neighbour search, gravity calculations, and cumulative neighbour search + gravity calculations for spherical Sobol distributions with up to 10^8 particles and ~ 105 neighbours per particle. For a given number of levels the RCB tree scales slightly better than $O(N)$, and the execution time only increases by a constant (the plot is shifted upwards) when another level is added to the tree. Overall, the execution time per particle increases much slower than the $\log(N)$ expected for standard tree codes. When increasing the particle number by a factor of 10^4 the execution time per particle increases merely by a factor of two.

and has been avoided whenever possible, usually by ‘revising’ the tree and amortising the cost of the tree build over a number of time steps. This, however, can become difficult: simulations involving black holes where particles are frequently absorbed at the horizon require a frequent tree build (if they orbit safely inside the horizon they can be temporarily stored in a special list and be removed only later, see Rosswog (2005), however at a substantial bookkeeping effort). Furthermore, since the tree build is usually the component of the code with the worst parallel scaling, having a fast tree build algorithm becomes crucial when parallelising the code. Therefore, the tree build is, together with the scaling behaviour close to $O(N)$, one of the strongest points of the RCB tree. The time for neighbour search takes 10-20%, the remaining 80-90% are invested for the gravitational forces.

In Fig. 15 we display the CPU time spent per particle in different parts of the code. This figure shows the $O(N)$ scaling of the neighbour search, even at 10^8 particles (the time spent searching the neighbours of one particle is always $\approx 13 \mu\text{s}$). At a given tree depth the gravity calculation scales slightly better than $O(N)$ for a given height of the tree (i.e., as more particles are added to the same cells, the CPU time per particle drops). This is partly an effect of the grouped tree traversal: since one tree walk and one ‘far force’ evaluation are performed per ll-cell, these two components of the code do not depend on the number of particles, but only on the height of the tree. This makes filling an ll-cell with more and more particles increasingly more efficient in terms of tree-traversals and far-gravity calculations (such behaviour can occur in any tree code, since adding one more level to a tree always increases the time needed by the tree walk, regardless of whether it is done per particle or per ll-cell). The near-gravity calculation, however, becomes more expensive since a larger number of particles is summed up directly. The total time per particle spent with tree operations is increasing somewhat, but at a much slower pace than the $\log(N)$ -behavior encountered for standard tree codes. When increasing the total particle number by a factor of 10^4 the time per particle merely increases by a factor of two.

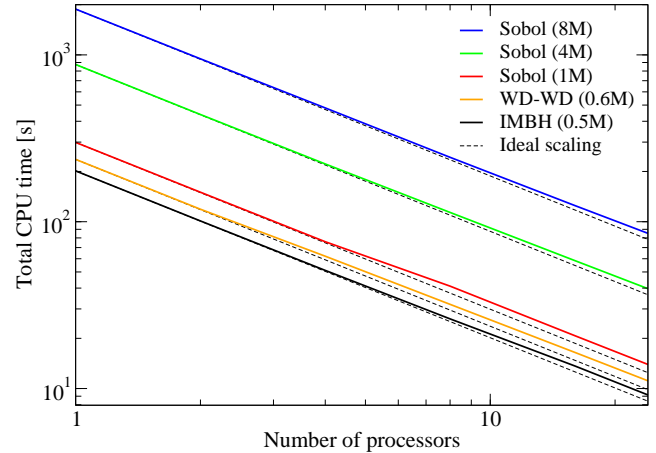


Figure 16. Scaling of the total CPU time (tree build + neighbour search + gravity calculations) with the number of processors. This plot also shows, with dashed lines, the ideal scaling for each of the five test cases. Not only are the results very close to the ideal scaling, but they improve as the number of particles N increases.

3.2.4 OpenMP parallelisation

The parallel code was compiled and executed on an SGI Altix 3700Bx2 machine with 24 Itanium2 processors (Madison9M) running at 1.6 GHz, with 6 MB of L2 cache and 96 GB of shared RAM. We tested the scaling of the RCB tree code with both the number of processors and particles. We chose three Sobol distributions (with 1, 4 and 8 million particles, respectively) and the two snapshot tests described above; the corresponding results are presented in Fig. 16. The results obtained in this test are rather robust against changes in the particle distribution and even particle number. In all cases a speedup of > 21 was obtained on 24 processors.

4 CONCLUSIONS

We have introduced a new tree for neighbour search and gravity that is based on recursive coordinate bisection. This binary RCB tree is only built down to an optimal depth so that there are still about 12 particles left per lowest-level cell. This property makes the tree fast (since some operations are only performed per lowest-level cell rather than per particle) and memory efficient since fewer aggregated quantities need to be stored for such a shallow tree. Gravity is split into a near- and far-field component; the first is calculated via a direct, kernel-smoothed summation while the latter uses a ‘cell-cell interaction’ based on Cartesian multipole and Taylor expansion.

We have compared the performance of our RCB tree against that of the ‘Press tree’ that we had used earlier on various occasions. As expected for such a ‘top-down’ tree, the tree building phase is substantially faster for RCB tree. At four million particles the tree build is faster by about a factor of 25, neighbour search and gravity (at slightly higher accuracy for the RCB tree) are faster by a factor of six. These ratios become even more favorable for the RCB tree with increasing particle numbers. The code was tested for up to 10^8 particles on a single processor, showing very good scaling behaviour close to $O(N)$ and a low memory consumption.

ACKNOWLEDGEMENTS

We would like to acknowledge useful discussions with Ivo Kabadshow from Forschungszentrum Jülich. This work was supported by Deutsche Forschungsgemeinschaft under grant number RO-3399/5-1. It has profited from visits to Oxford which were supported by a DAAD grant ‘Projektbezogener Personenaustausch mit Großbritannien’ under grant number 313-ARC-XXIII-Ik and from visits to La Scuola Internazionale Superiore di Studi Avanzati (SISSA), Trieste, Italy. It is a pleasure to acknowledge in particular the hospitality of John Miller (Oxford, Trieste). We gratefully acknowledge the hospitality of the University of Basel (E.G.) and the University of Queensland in Brisbane (S.R.) during the time when this paper was finalized. S.R.’s stay in Brisbane was supported by the DFG by a grant to initiate and intensify bilateral collaboration.

REFERENCES

- Anderson R. J., 1993, in Silver Jubilee Workshop on Computing and Intelligent Systems Computer science problems in astrophysical simulation. pp 48–61
- Anderson R. J., 1999, *SIAM J. Comput.*, 28, 1923
- Bagla J. S., 2002, *Journal of Astrophysics and Astronomy*, 23, 185
- Bagla J. S., Ray S., 2003, *New Astronomy*, 8, 665
- Barnes J., Hut P., 1986, *Nature*, 324, 446
- Bate M. R., Bonnell I. A., Price N. M., 1995, *MNRAS*, 277, 362
- Bentley J., 1975, *Communications of the ACM*, 18, 509
- Benz W., Bowers R., Cameron A., Press W., 1990, *ApJ*, 348, 647
- Benz W., Thielemann F.-K., Hills J. G., 1989, *ApJ*, 342, 986
- Bode P., Ostriker J. P., Xu G., 2000, *ApJS*, 128, 561
- Bonnell I. A., Bate M. R., Vine S. G., 2003, *MNRAS*, 343, 413
- Cormen T. H., Leiserson C. E., Rivest R. L., Stein C., 2001, *Introduction to Algorithms*. The MIT Press, New York
- Couchman H. M. P., 1991, *ApJ*, 368, L23-L26
- Couchman H. M. P., Thomas, P. A. and Pearce, F. R., 1995, *ApJ*, 452, 797
- Dachsel H., 2010, *J. Chem. Phys.*, 132, 119901
- Dan M., Rosswog S., Guillochon J., Ramirez-Ruiz E., 2011, submitted to *ApJ*, p. X
- Dehnen W., 2000, *ApJL*, 536, L39
- Dehnen W., 2001, *MNRAS*, 324, 273
- Dehnen W., 2002, *J. Comput. Phys.*, 179, 27
- Dubinski J., 1996, *New Astronomy*, 1, 133
- Dyer C. C., Ip P. S. S., 1993, *ApJ*, 409, 60
- Efstathiou G., Davis M., White S. D. M., Frenk C. S., 1985, *ApJ*, 57, 241
- Evrard A. E., 1988, in N. Kaiser & A. N. Lasenby ed., *Post-Recombination Universe Extending N-body methods with SPH*. pp 363–366
- Greengard L., Rokhlin V., 1987, *J. Comput. Phys.*, 73, 325
- Hernquist L., 1987, *ApJS*, 64, 715
- Hernquist L., Katz N., 1989, *ApJS*, 70, 419
- Hoare C., 1962, *Computer Journal*, 5, 10
- Hockney R. W., Eastwood J. W., 1988, *Computer Simulation Using Particles*, 1. edn. McGraw-Hill, New York
- Macfarland T., Couchman H. M. P., Pearce F. R., Pichlmeier J., 1998, *New Astron.*, 3, 687
- Makino J., 1990, *J. Comput. Phys.*, 88, 393
- Merlin E., Buonomo U., Grassi T., Piovani L., Chiosi C., 2010, *A & A*, 513, A36+
- Monaghan J., Lattanzio J., 1985, *A&A*, 149, 135
- Monaghan J., 2002, *MNRAS*, 335, 843
- Nelson A. F., Wetzstein M., Naab T., 2009, *ApJS*, 184, 326
- Press W. H., 1986, in P. Hut & S. L. W. McMillan ed., *The Use of Supercomputers in Stellar Dynamics Vol. 267 of Lecture Notes in Physics*, Berlin Springer Verlag, Techniques and Tricks for N-Body Computation. p. 184
- Press W. H., Flannery B. P., Teukolsky S. A., Vetterling W. T., 1992, *Numerical Recipes*. Cambridge University Press, New York
- Price D., Monaghan J., 2007, *MNRAS*, 374, 1347
- Price D., Rosswog S., 2006, *Science*, 312, 719
- Price D., 2007, *Publications of the Astronomical Society of Australia*, 24, 159
- Price D., Bate M. R., 2009, *MNRAS*, 398, 33
- Rosswog S., 2005, *ApJ*, 634, 1202
- Rosswog S., Ramirez-Ruiz E., Hix W. R. & Dan M., 2008, *Computer Physics Communications*, 179, 184
- Rosswog S., 2009, *New Astronomy Reviews*, 53, 78
- Rosswog S., Davies M. B., 2002, *MNRAS*, 334, 481
- Rosswog S., Kasen D., Guillochon J., Ramirez-Ruiz E., 2009, *ApJL*, 705, L128
- Rosswog S., Liebendörfer M., Thielemann F.-K., Davies M., Benz W., Piran T., 1999, *A & A*, 341, 499
- Rosswog S., Price D., 2007, *MNRAS*, 379, 915
- Rosswog S., Ramirez-Ruiz E., Hix R., 2009, *ApJ*, 695, 404
- Salmon J. K., Warren M. S., 1994, *J. Comput. Phys.*, 111, 136
- Springel V., 2005, *MNRAS*, 364, 1105
- Springel V., Hernquist L., 2002, *MNRAS*, 333, 649
- Stadel J. G., 2001, PhD thesis, University of Washington
- Thacker R. J., Couchman H. M. P., 2006, *Comput. Phys. Commun.*, 174, 540
- Turner J. A., Chapman S. J., Bhattal A. S., Disney M. J., Pongracic H., Whitworth A. P., 1995, *MNRAS*, 277, 705
- Wadsley J. W., Stadel J. & Quinn T., 2004, *New Astronomy*, 9, 137
- Waltz J., Page G. L., Milder S. D., Wallin J., Antunes A., 2002, *J. Comput. Phys.*, 178, 1
- Xu G., 1995, *ApJS*, 98, 355

This paper has been typeset from a \LaTeX file prepared by the author.